INSTITUTE OF PHYSICS PUBLISHING SEMICONDUCTOR SCIENCE AND TECHNOLOGY
Semicond. Sci. Technol. **17** (2002) 860–869 PII: S0268-1242(02)37916-1

Band anticrossing in highly mismatched III–V semiconductor alloys

J Wu[1,2], **W Shan**[3] **and W Walukiewicz**[2]

[1] Applied Science and Technology Graduate Group, University of California, Berkeley, CA 94720, USA
[2] Materials Sciences Division, Lawrence Berkeley National Laboratory, Berkeley, CA 94720, USA
[3] OptiWork, Inc., Fremont, CA 94538, USA

Received 29 March 2002
Published 12 July 2002
Online at stacks.iop.org/SST/17/860

Abstract
In this paper we review the basic theoretical aspects as well as some important experimental results of the band anticrossing effects in highly electronegativity-mismatched semiconductor alloys, such as $GaAs_{1-x}N_x$ and $In_yGa_{1-y}As_{1-x}N_x$. The many-impurity Anderson model treated in the coherent potential approximation is applied to these semiconductor alloys, in which metallic anion atoms are partially substituted by a highly electronegative element at low concentrations. Analytical solutions of the Green's function provide dispersion relations and state broadenings for the restructured conduction bands. The solutions also lead to the physically intuitive and widely used two-level band anticrossing model. Significant experimental observations, including large bandgap reduction, great electron effective mass enhancement and unusual pressure behaviour of the bandgap, are compared with the predictions of the band anticrossing model. The band anticrossing model is extended over the entire Brillouin zone to explain the pressure behaviour of the lowest conduction band minimum in $GaP_{1-x}N_x$. Finally, we show that the band anticrossing can also account for the large bandgap bowing parameters observed in $GaAs_xSb_{1-x}$, $InAs_ySb_{1-y}$ and GaP_xSb_{1-x} alloys.

1. Introduction

The understanding of the electronic structure of random semiconductor alloys has been one of the interesting and important areas of semiconductor research for a long time. The simplest treatment of such alloys is the virtual crystal approximation (VCA) that is applicable to perfectly random alloys [1, 2]. In this approximation, the electronic properties of the alloys are given by the linear interpolation between the properties of the end-point materials. The alloy disorder effects are typically included through a bowing parameter that describes the deviations from the VCA. Most of the studies of semiconductor alloy systems are restricted to the cases where there are only small differences between properties of the end-point semiconductors. Such 'well-matched' alloys can be easily synthesized and their properties are close to the VCA predictions.

Recent progress in the epitaxial growth techniques has led to the successful synthesis of semiconductor alloys composed of materials with distinctly different properties. The properties of these 'highly mismatched' alloys (HMAs) deviate drastically from the predictions of the VCA. The most prominent class of HMAs comprises the III–V_{1-x}–N_x alloys, in which highly electronegative nitrogen substitutes group V anions in group III–V compounds. Nitrogen incorporation into III–V semiconductors results in numerous effects, such as a dramatic reduction in the fundamental bandgap [3], an increase in the electron effective mass [4] and a significant decrease in the electron mobility [5].

The most striking and practically important feature of the HMAs was a large bandgap reduction. For example, it has been found that incorporation of only 1% of N into GaAs reduces the energy gap by about 180 meV [3]. Similarly, large bandgap reductions were also observed in other group III–V_{1-x}–N_x alloys [6–9]. The first attempts to explain this unusual behaviour were based on a dielectric model that predicted highly nonlinear composition dependencies

of the bandgap for the alloys of semiconductor compounds with very different properties [10]. The model predicted a semiconductor to semi-metal transition in some of the alloys [11]. The large bandgap reduction in GaN_xAs_{1-x} alloys has also been explained by Wei and Zunger [12] in terms of a large composition dependent bowing parameter that could be decomposed into three different contributions: a volume deformation, a charge exchange and a structural relaxation. This approach was abandoned later and several other theoretical explanations of the large bandgap reduction in III–V–N alloys have also been proposed [13–17].

Alternatively, the band structures of HMAs have been explained in terms of the two-level band anticrossing (BAC) model. The BAC model has been developed to explain the pressure and composition dependencies of the bandgap of $In_yGa_{1-y}As_{1-x}N_x$ alloys [18]. Later it was successfully applied to other HMAs [19, 20]. Furthermore, it has predicted several new effects, such as a N-induced enhancement of the electron effective mass [4], an improvement in the donor activation efficiency [21] in $In_yGa_{1-y}As_{1-x}N_x$ alloys and the change in the nature of the fundamental bandgap from indirect to direct in $GaP_{1-x}N_x$ [20]. In the meantime, all these predictions have been experimentally confirmed.

In the BAC model, the restructuring of the conduction band is a result of an anticrossing interaction between highly localized A_1 states of the substitutional N atoms and the extended states of the host semiconductor matrix. The newly formed sub-bands, named E_+ and E_-, have dispersion relations given by [18]

$$E_\pm(k) = \tfrac{1}{2}\left\{[E^C(k) + E^L] \pm \sqrt{[E^C(k) - E^L]^2 + 4V^2 \cdot x}\right\}, \tag{1}$$

where $E^C(k)$ is the energy dispersion of the lowest conduction band of the host, and E^L is the energy of the localized states derived from the substitutional N atoms. The coupling between the localized states and the band states of the host is described by the adjustable parameter V. The BAC model provides a simple, analytical expression to calculate the electronic and optical properties of III–V_{1-x}–N_x alloys.

The two-level BAC model is a natural result of degenerate perturbation theory applied to a system of localized states and extended states. The interaction between these two types of states has been treated in the simplest possible manner that does not account for expected severe level broadening effects. It is enlightening to notice the similarities between this localized extended hybridization problem and the s–d exchange interaction for a single-impurity atom of a transition metal or a rare-earth element in a non-magnetic metal. The single-site Anderson model has been developed to describe the latter. In Anderson's s–d exchange model [22], the electron system is separated into a delocalized part of the matrix metal that is described in terms of band theory, and a localized level of the d-shell electrons of the impurity atom. A dynamical mixing term is introduced into the Hamiltonian of the system to describe the hybridization between the band states and the localized impurity states. While solving the Anderson Hamiltonian, it has been found that, as a result of the hybridization, the impurity d-state becomes a virtual energy state with an imaginary energy part proportional to the strength of the s–d hybridization. The imaginary part of the eigen-energy of the virtual state defines the width of the density redistribution of the d-state, and determines the lifetime of the state before the d-electrons are delocalized into the band states through the exchange interaction.

A many-impurity Anderson model has been proposed to describe the electronic properties of semiconductor crystals with low concentrations of deep-level transition-metal impurities [23, 24]. Very recently, the many-impurity Anderson model has also been used to evaluate the interaction between the randomly distributed localized states and the extended states in HMAs [25]. The calculations have reproduced the two-level BAC model results for the restructuring of the conduction band. The imaginary part of the Green's function also yields new information on the electronic level broadening that is used to determine the broadening of the optical transitions and to calculate the free electron mobility.

In this paper, the theoretical aspects of the BAC model are reviewed on the basis of the many-impurity Anderson model. Comparisons are made between important theoretical results and basic experimental observations for III–V_{1-x}–N_x alloys. The basic BAC model is also extended to the entire Brillouin zone to explain new experimental findings.

2. Theory

2.1. Band restructuring: many-impurity Anderson model in the coherent potential approximation

Hjalmarson *et al* were the first to predict that the incorporation of isoelectronic impurities into semiconductors gives rise to highly localized impurity states [26]. The energy of these states largely depends on the electronegativity of the substitutional impurity. In the case of highly electronegative impurities substituting metallic anions in compound semiconductors, the energy levels are located close to the conduction band edge [26]. For example, substitutional nitrogen, an isoelectronic impurity in GaAs, generates an A_1-symmetry level located at ∼0.23 eV above the conduction band edge of GaAs resonant with the conduction band. This resonant level has been observed in optical experiments when it is moved into the GaAs bandgap by applying hydrostatic pressure [27] or alloying with GaP [28]. With increasing N impurity concentration, the interaction between the localized N levels and the GaAs band states changes the electronic structure of the resulting $GaAs_{1-x}N_x$ system.

The electronic structure of HMAs (e.g., $GaAs_{1-x}N_x$) can be described by considering an interaction between the localized states ($|L\rangle$) and extended states ($|\mathbf{k}\rangle$) within the many-impurity Anderson model. The total Hamiltonian of the system is the sum of three terms [23, 24],

$$H = \sum_{\mathbf{k}} E^C_{\mathbf{k}} c^+_{\mathbf{k}} c_{\mathbf{k}} + \sum_j E^L_{\mathbf{j}} d^+_{\mathbf{j}} d_{\mathbf{j}} + \frac{1}{\sqrt{N}} \sum_{j,\mathbf{k}} (e^{i\mathbf{k}\cdot\mathbf{j}} V_{\mathbf{kj}} c^+_{\mathbf{k}} d_{\mathbf{j}} + \text{h.c.}), \tag{2}$$

where the first term is the Hamiltonian of the electrons in the band states with energy dispersion $E^C_{\mathbf{k}}$, and the second term corresponds to the total energy of electrons localized on impurity sites. The third term describes the change in the

single electron energy due to the dynamical mixing between the band states and the localized states. It is assumed that only one band and one impurity level are involved in the process. Following Anderson's scheme, the hybridization strength is characterized by the parameter $V_{\mathbf{kj}}$ defined by the following equation [22],

$$\begin{aligned}\langle \mathbf{k}|H_{\mathrm{HF}}|L\rangle &= \frac{1}{\sqrt{N}}\sum_{l,j} \mathrm{e}^{\mathrm{i}\mathbf{k}\cdot\mathbf{l}} \int a^*(\mathbf{r}-\mathbf{l})H_{\mathrm{HF}}(\mathbf{r})\varphi_L(\mathbf{r}-\mathbf{j})\,\mathrm{d}\mathbf{r} \\ &= \frac{1}{\sqrt{N}}\sum_{j} \mathrm{e}^{\mathrm{i}\mathbf{k}\cdot\mathbf{j}} \cdot \sum_{l} \mathrm{e}^{\mathrm{i}\mathbf{k}(\mathbf{l}-\mathbf{j})} \\ &\quad \times \int a^*(\mathbf{r}-\mathbf{l})H_{\mathrm{HF}}(\mathbf{r})\varphi_L(\mathbf{r}-\mathbf{j})\,\mathrm{d}\mathbf{r} \\ &\equiv \frac{1}{\sqrt{N}}\sum_{j=1} \mathrm{e}^{\mathrm{i}\mathbf{k}\cdot\mathbf{j}} V_{\mathbf{kj}}, \end{aligned} \tag{3}$$

where $a(\mathbf{r}-\mathbf{l})$ and $\varphi_L(\mathbf{r}-\mathbf{j})$ are the Wannier function belonging to the band and the localized wavefunction of the impurity on the jth site, respectively. $H_{\mathrm{HF}}(\mathbf{r})$ is the single electron energy described in the Hartree–Fock approximation.

When there is only one impurity atom present, the model reduces to the original Anderson model. In general, one could consider finite but dilute concentrations of impurities, $0 < x \ll 1$. Assuming that the impurities are randomly distributed in space, one can carry out a configurational averaging, neglecting correlations between positions of the impurities. The coherent potential approximation (CPA) is usually used to treat such systems [29, 30]. In the CPA, consecutive multiple scatterings from each single-impurity atom are fully taken into account, but correlations between scatterings from different impurity atoms are neglected due to the lack of coherence between the randomly distributed impurity sites. After the configurational averaging in the frame of CPA, the average Green's function restores the space translational invariance, and $\mathbf{k}$ resumes its well-defined properties as a good quantum number. In momentum space, the diagonal Green's function can be written as [23, 29, 30]

$$G_{\mathbf{kk}}(E) = \left[E - E^C_{\mathbf{k}} - \frac{V^2 x}{E - E^L - \mathrm{i}\pi\beta V^2 \rho_0(E^L)}\right]^{-1}, \tag{4}$$

where V is the average value of $V_{\mathbf{kj}}$, assuming weak dependencies on $\mathbf{k}$ and $\mathbf{j}$, and ρ_0 is the unperturbed density of states of $E^C_{\mathbf{k}}$ per unit cell. Since ρ_0 only weakly depends on energy, it can be assumed to be a constant in the lowest order approximation, with an effective value equal to the unperturbed density of states evaluated at E^L and multiplied by a prefactor β. The new dispersion relations are determined by the poles of $G_{\mathbf{kk}}(E)$, and the solutions are given by an equivalent two-level-like eigenvalue problem,

$$\begin{vmatrix} E^C_{\mathbf{k}} - E(\mathbf{k}) & V\sqrt{x} \\ V\sqrt{x} & E^L + \mathrm{i}\Gamma_L - E(\mathbf{k}) \end{vmatrix} = 0, \tag{5}$$

where $\Gamma_L = \pi\beta V^2 \rho_0(E^L)$ is the broadening of E^L in the original single-impurity Anderson model [22].

2.2. *Simplified representation: two-level band anticrossing model*

If $\Gamma_L = 0$, equation (5) is reduced to the two-level BAC model of equation (1) with two restructured dispersions for the upper and lower conduction sub-bands. The flattened and downshifted lower sub-band is responsible for most of the unusual effects, such as the drastic bandgap reduction and the electron effective mass enhancement. These effects will be addressed in section 3 of the paper.

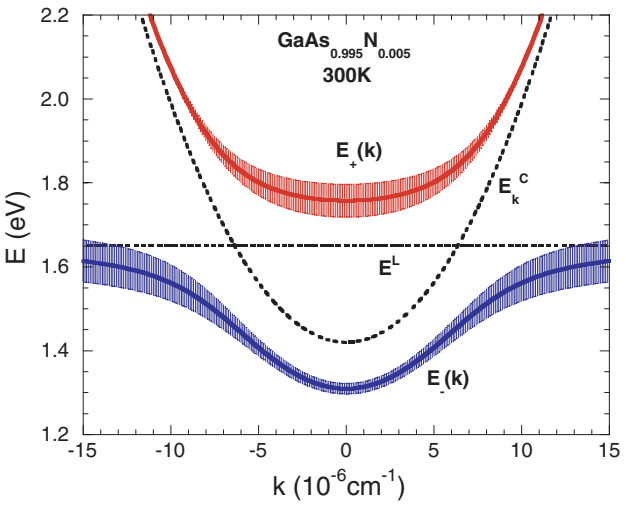

Figure 1. Conduction band restructuring according to equation (1) for $GaAs_{0.995}N_{0.005}$. The broadening of the dispersion curves of the newly formed sub-bands illustrates the energy uncertainties defined in equation (7). All the energies are referenced to the top of the valence band of GaAs.

When the broadening Γ_L is nonzero but small, so that $2V\sqrt{x} \gg \pi\beta V^2\rho_0(E^L)$ and $\left|E^C_{\mathbf{k}} - E^L\right| \gg \pi\beta V^2\rho_0(E^L)$, one obtains an approximate analytical solution for equation (5),

$$\begin{aligned}\tilde{E}_{\pm}(\mathbf{k}) &\approx E_{\pm}(\mathbf{k}) + \mathrm{i}\Gamma_L \frac{\left[E_{\pm}(\mathbf{k}) - E^C_{\mathbf{k}}\right]}{\left[E_{\pm}(\mathbf{k}) - E^C_{\mathbf{k}}\right] + \left[E_{\pm}(\mathbf{k}) - E^L\right]} \\ &\equiv E_{\pm}(\mathbf{k}) + \mathrm{i}\Gamma_{\pm}(\mathbf{k}), \end{aligned} \tag{6}$$

where $E_{\pm}(\mathbf{k})$ is the real part of $\tilde{E}_{\pm}(\mathbf{k})$ and is defined in equation (1). The imaginary part of the dispersion relations defines the hybridization-induced energy uncertainties. It is worth noticing that the imaginary part in equation (6) is proportional to the admixture of the localized states to the restructured wavefunctions in the two-level-perturbation picture described by equation (5),

$$\Gamma_{\pm}(\mathbf{k}) = |\langle L|E_{\pm}(\mathbf{k})\rangle|^2 \cdot \Gamma_L. \tag{7}$$

As an example, figure 1 shows the schematic dispersion relations for the sub-bands given by equation (1) for $GaAs_{0.995}N_{0.005}$ near the Brillouin zone centre. The broadenings of the dispersion relations are given by the imaginary part of equation (6).

We note that the original Anderson Hamiltonian (equation (2)) and the coherent potential approximation ignore interactions between neighbouring impurity states. The spatial distribution of the impurity atoms is assumed random and homogeneous. The application of this model is in principle limited to dilute impurity concentrations for which the distance between neighbouring impurity atoms is much larger than the spatial extension of the impurity wavefunction (e.g., the wavefunction of the N resonant states). The nitrogen cluster luminescence has been experimentally observed in $GaAs_{1-x}N_x$ at dilute N concentrations [31]. It should be emphasized

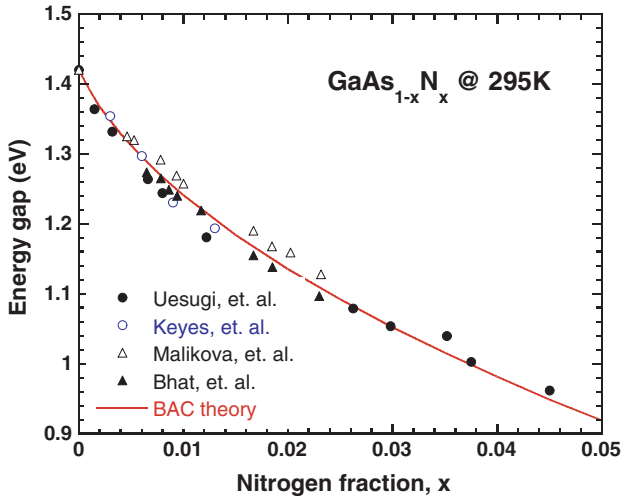

Figure 2. Energy gap of $GaAs_{1-x}N_x$ as a function of N concentration from various reports [3, 31–33]. The solid curve is the fitting of the BAC model.

however that the observation of photoluminescence lines attributed to specific N clusters does not imply that the concentration of such clusters is large enough to significantly change the concentration of the isolated N atoms and affect the conclusions based on the BAC model. It has been shown previously that small inter-impurity interaction effects may be accounted for within the BAC model by assuming that $E^C_{\mathbf{k}}$, E_L and the coupling parameter depend on the N concentration [32].

3. Comparison with experiment

3.1. Fundamental energy gap

The bandgap reduction in $GaAs_{1-x}N_x$ alloys is accounted for by the downward shift of the conduction band edge caused by the anticrossing interaction. Figure 2 shows the fundamental bandgap as a function of N concentration from various reports [3, 33–35] together with the dependence calculated from equation (1). The best fit is obtained with an interaction constant of $V = 2.7\,\mathrm{eV}$.

The additional E_+ transition at energies blue-shifted from the previously observed N resonant level [18] suggests a strong interaction between the N states and the host GaAs. Figure 3(*a*) shows the photomodulated reflectance (PR) spectra for $GaAs_{1-x}N_x$ for a range of N concentrations [36]. The critical energies are plotted as a function of x in figure 3(*b*). In figure 3(*b*) it can be seen that the spin–orbit transition energy $E_- + \Delta_0$ follows E_-, indicating that the top of the valence band of GaAs is not affected by the N incorporation. The symmetric shift of E_+ and E_- is a typical behaviour for interacting two-level systems. On the other hand, the E_1 energy that corresponds to the inter-band transition along the Λ line in the Brillouin zone, exhibits a much weaker composition dependence. This implies that away from the Brillouin zone centre, the effect of N incorporation on the band structure of GaAs is much weaker.

The anticrossing character of E_+ and E_- is not only reflected in the composition dependence, but also manifested

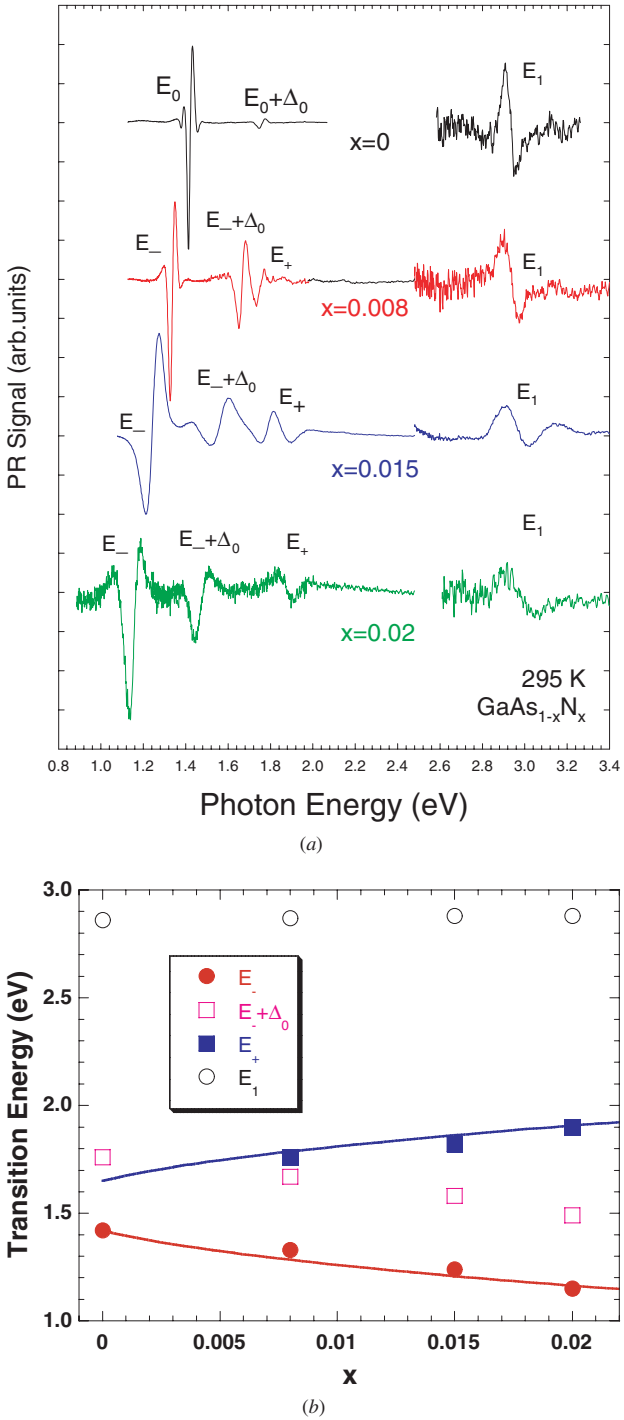

Figure 3. (*a*) Photomodulated reflectance spectra showing the critical transitions. (*b*) The critical energies obtained from (*a*) plotted as a function of x.

in their pressure dependencies. Figure 4 shows the energy position of the E_+ and E_- transitions for $GaAs_{0.985}N_{0.015}$ as a function of hydrostatic pressure [36]. The solid curves represent the pressure dependencies calculated from equation (1), using previously known pressure coefficients $\mathrm{d}E^C/\mathrm{d}P = 10.8\,\mathrm{meV\ kbar^{-1}}$ for the GaAs conduction band edge, and $\mathrm{d}E^L/\mathrm{d}P = 1.5\,\mathrm{meV\ kbar^{-1}}$ for the N-localized states.

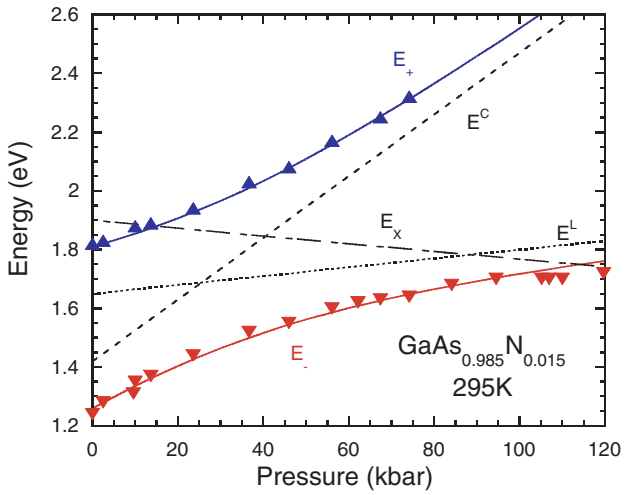

Figure 4. Energies of the E_+ and E_- transitions obtained from PR experiments as a function of hydrostatic pressure for $GaAs_{0.985}N_{0.015}$.

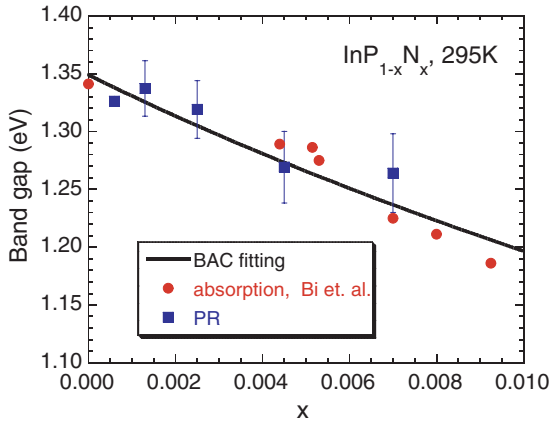

Figure 5. Energy gap of $InP_{1-x}N_x$ as a function of x. The solid line is a fit based on the BAC model.

Similar band anticrossing effects have also been observed in several other N-containing III–V alloys, such as $GaP_{1-x}N_x$ [6], $InP_{1-x}N_x$ [7], $GaSb_yAs_{1-x-y}N_x$ [8] and $InSb_{1-x}N_x$ [9]. Shown in figure 5 is the bandgap bowing of $InP_{1-x}N_x$ grown by gas-source molecular beam epitaxy with small N concentrations [37]. The energy of the localized N-level $E^L = 2.0$ eV above the valence band edge of InP was estimated from the valence band offset of 0.35 eV between InP and GaAs. A BAC fitting leads to a coupling constant of $V = 3.5$ eV in $InP_{1-x}N_x$.

3.2. *BAC effects in $GaAs_{1-x}N_x$/GaAs quantum wells*

The band anticrossing interaction also has significant effects on the optical transitions in $GaAs_{1-x}N_x$/GaAs quantum wells (QW). Since the perturbation of N on the band structure of GaAs is mainly in the lowest conduction band, it can be expected that the band offset between $GaAs_{1-x}N_x$ and GaAs is mostly in the conduction band. Indeed, photoluminescence [38] and x-ray photoelectron spectroscopy [39] studies of $GaAs_{1-x}N_x$/GaAs heterostructures indicate a slightly type-II

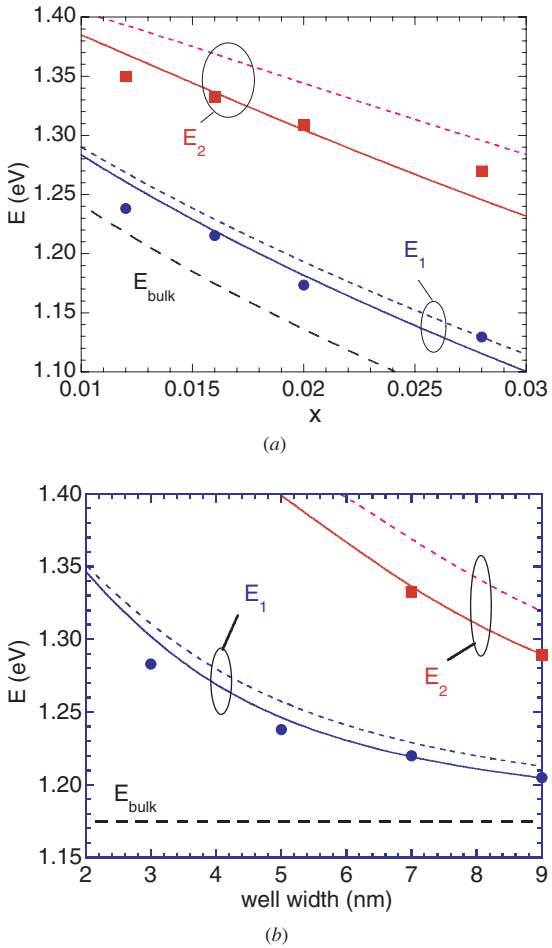

Figure 6. (*a*) First and second transition energies as a function of N concentration for $GaAs_{1-x}N_x$/GaAs QWs with 7 nm well width. Solid curves: calculated values using the BAC model with the $GaAs_{1-x}N_x$ electron effective mass given by equation (8); Short dashed curves: calculated values assuming the $GaAs_{1-x}N_x$ electron effective mass is equal to m^*_{GaAs}. Long dashed curve: bandgap of bulk $GaAs_{1-x}N_x$ given by the BAC model. (*b*) The transition energies as a function of well width for $x = 0.016$. The different types of curves represent the same calculations respectively as in (*a*).

band lineup with a very small negative valence-band offset of $|\Delta E_V| < 20\,\text{meV}/\%\text{N}$.

The inter-band optical transitions in $GaAs_{1-x}N_x$/GaAs multiple QWs have been measured by PR experiments [40]. Figure 6(*a*) shows the transition energies as a function of the N concentration for a 7 nm multiple QW with 20 nm GaAs barriers. These energies, denoted as E_1 and E_2, are attributed to the critical transitions from the valence band edge to the ground state and first excited state, respectively, in the confined E_- sub-band. To understand the composition dependence quantitatively, we have applied a finite-depth single-square-well model to calculate the confinement energies. The well depth for the confined electrons in the $GaAs_{1-x}N_x$ layer is given by the downward shift of the conduction band determined by equation (1). The effective mass inside the well is approximated by the density-of-state electron effective mass evaluated at the Brillouin zone centre,

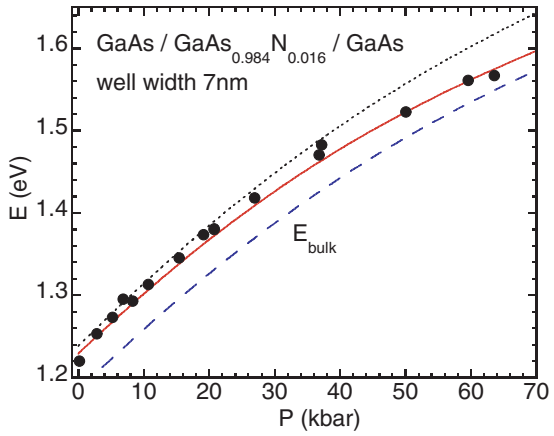

Figure 7. The first transition energy, E_1, as a function of hydrostatic pressure for $x = 0.016$ and well width = 7 nm. The different types of curves have the same meanings as in figure 6.

$$m^* \approx \hbar^2 \left| \frac{k}{\mathrm{d}E_-(k)/\mathrm{d}k} \right|_{k=0} = 2m^*_{\mathrm{GaAs}} \Bigg/ \left[1 - \frac{E^C(0) - E^L}{\sqrt{(E^C(0) - E^L)^2 + 4V^2 x}} \right]. \quad (8)$$

The effective mass calculated in equation (8) increases rapidly with x from $m^*_{\mathrm{GaAs}} = 0.067m_0$ for pure GaAs to about $0.1m_0$ at $x = 0.01$. The solid curves in figure 6(a) are the calculated transition energies assuming a composition dependence of the effective mass given by equation (8). To illustrate the effect of the heavier electron mass in the QW, we have also calculated the optical transition energies assuming that the effective mass of $GaAs_{1-x}N_x$ is unchanged from that of GaAs. The results are shown as short-dashed curves in figure 6(a). Evidently, much better agreement with the experiment is obtained when the effect of mass enhancement is taken into account. It is also necessary to include the heavier mass effect to explain the well width dependence of the transition energies. Figure 6(b) shows E_1 and E_2 as a function of the well width for a constant N concentration of $x = 0.016$.

The pressure dependence of the transition energy further supports the conclusion of heavier electron mass in the well layer. In figure 7 E_1 is shown as a function of hydrostatic pressure for a QW. At high pressures, the experimental data-points deviate from the predicted values based on the assumption of constant effective mass, and can only be accommodated by the heavier mass calculations. It should be noted that with the increasing pressure, the electron effective mass is further increased as a result of the stronger flattening of $E_-(k)$. For example, for $x = 0.016$, the mass increases from $0.11m_0$ at ambient pressure to $0.28m_0$ at 70 kbar, two fold enhanced from the electron effective mass of the GaAs host. Similar increases in the effective mass of $GaAs_{1-x}N_x$ have been reported using various experimental techniques [41, 42].

3.3. Band anticrossing in the entire Brillouin zone

It has been demonstrated that the incorporation of N into GaP changes the nature of the fundamental bandgap from indirect to direct [20]. A new conduction band minimum is formed at the Γ point as a result of the anticrossing between the Γ edge

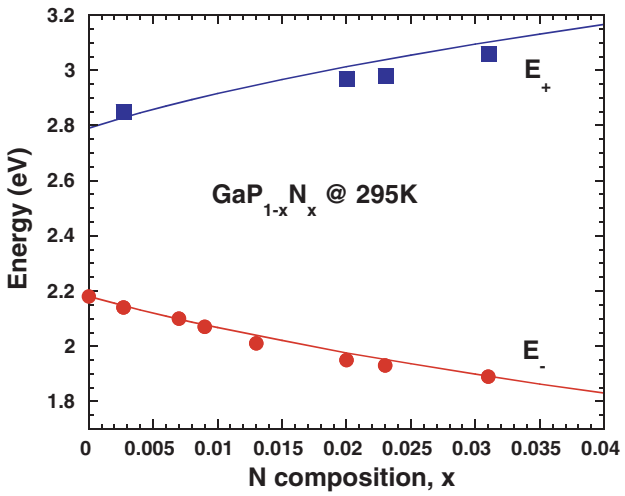

Figure 8. E_+ and E_- measured by PR as a function of x for $GaP_{1-x}N_x$.

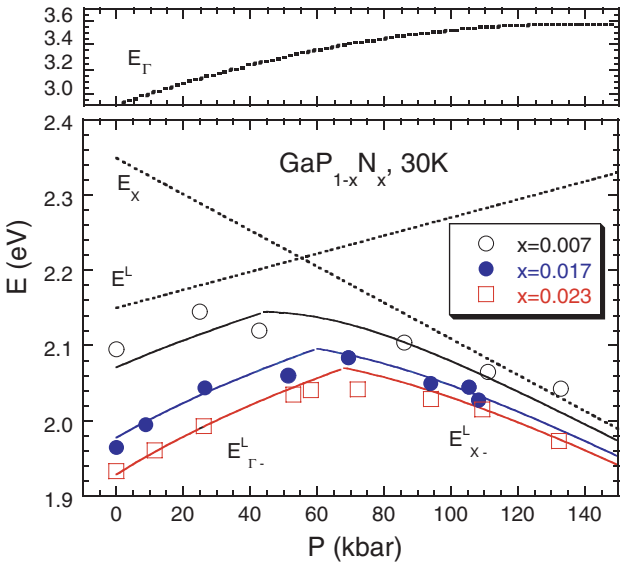

Figure 9. Photoluminescence peak energy at 30 K as a function of pressure for three samples with different N concentrations. The dashed lines indicate the pressure dependencies of the N-localized state, the Γ band and the X band minima of GaP. The solid curves are the calculated lowest conduction band energies for the three N concentrations based on the BAC model.

of the conduction band and the N level, which is located at 2.15 eV above the top of the valence band. The interaction strength has been determined to be $V = 3.05$ eV. Figure 8 shows the energies of E_- and E_+ observed using PR spectroscopy as a function of N concentration, in comparison with the BAC calculations.

Since the wavefunction of N states is highly localized in real space, its Fourier transform has significant contributions by off-zone-centre components in the Brillouin zone. It is, therefore, expected to couple not only to the Γ conduction state, but also to other conduction states such as the L and X band minima. We have investigated the hydrostatic pressure dependence of the fundamental bandgap of $GaP_{1-x}N_x$ alloys using photoluminescence (PL) technique at low temperature (30 K) [43]. Our results are summarized in figure 9. It can be

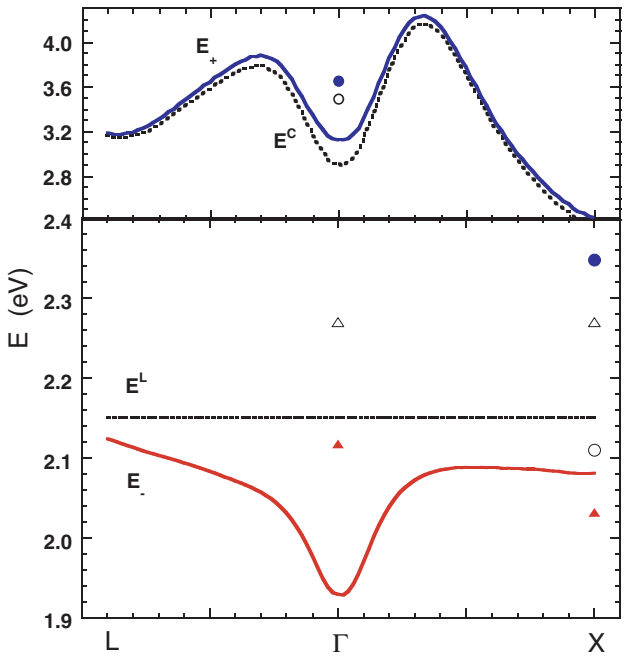

Figure 10. BAC-induced restructuring of the conduction band of $GaP_{1-x}N_x$. The curves show the lower $E_-(k)$ and the upper $E_+(k)$ bands at ambient pressure. The symbols show the energy minima at 100 kbar: open triangles, N-localized level E^L; open circles, E^C (including E_Γ and E_X); solid triangles, E_- (including $E^L{}_{\Gamma-}$ and $E^L{}_{X-}$); solid circles, E_+ (including $E^L{}_{\Gamma+}$ and $E^L{}_{X+}$). Note the change in the nature of the lowest conduction band edge, from direct at ambient pressure to indirect, mostly X-like at 100 kbar.

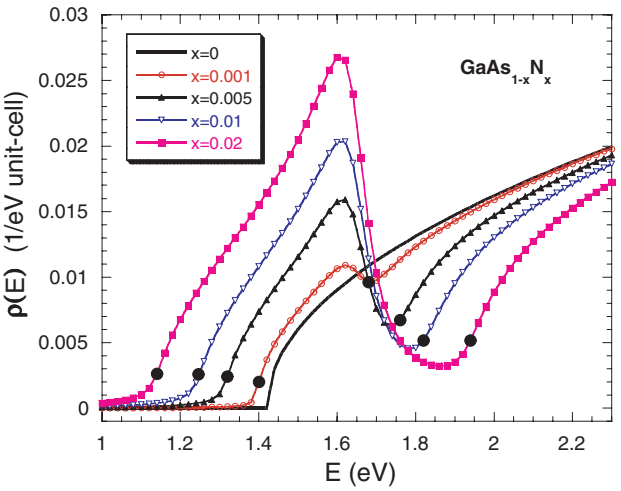

Figure 11. Density of states of $GaAs_{1-x}N_x$ alloys for a range of values of x as compared with the unperturbed density of states. The two black dots on each curve indicate the energy positions of the E_- and E_+ sub-band edges.

seen that at high pressures, the fundamental bandgap shifts to lower energy, approaching the negative pressure dependency of the X band minimum of GaP. The non-monotonic pressure dependence of the fundamental bandgap is explained by the interactions of the N-localized states with the Γ band edge of GaP at low pressures and with the X band edge at high pressures. The interaction constant is determined to be $V = 0.90$ eV at the X point, indicating a much weaker coupling than at the Γ point.

Evidence of similar off-zone-centre coupling in $GaAs_{1-x}N_x$ alloy has been observed by Seong *et al* using resonant Raman scattering [44] and by Perkins *et al* using electroreflectance technique [45]. In these ambient-pressure experiments, a coupling between N states and the conduction band edge at the L point of the Brillouin zone was observed. This is because in GaAs, the N level is closer to the L band minima (separation = 0.12 eV) than to the X minima (separation = 0.27 eV), whereas in GaP it is located much closer to the X band minima than to the L minima, with separations equal to 0.17 eV and 0.46 eV, respectively. In GaAs, the negative pressure derivative resulting from the coupling between E^L-localized levels and E_X minima can be observed only at very large pressures when the X band minima are shifted down to the band edge. In fact, the onset of this effect has shown up in $GaAs_{1-x}N_x$ at a pressure of about 100 kbar, as can be seen in figure 4. Shown in figure 10 is a schematic diagram of the conduction bands of $GaP_{0.977}N_{0.023}$ at ambient pressure. In the calculation, $V(k)$ is assumed to take the functional form of the Fourier transform of an exponentially decaying function, specifically [25],

$$V(k) = \frac{V_\Gamma}{[1 + (ak)^2]^2}. \tag{9}$$

In equation (9), a is a parameter describing the spatial extent of the N localized wavefunction, and has been estimated to be of the order of the lattice constant of the host, so that V_X agrees with the value determined from the X–N anticrossing fitting. The energy minima restructured from the Γ–N and X–N anticrossing interactions at 100 kbar are also shown as symbols in figure 10. The fundamental bandgap of the material switches from direct at ambient pressure to indirect at high pressures.

3.4. State broadening and related effects

It is interesting to see the effects of band anticrossing on the density of states of the conduction band. The original density of states per unit cell for the GaAs conduction band edge is assumed to have a parabolic form following the effective-mass theory,

$$\rho_0(\varepsilon) = 4\pi\sqrt{\varepsilon - E_0^C}\,/\varepsilon_B^{3/2}, \tag{10}$$

where $\varepsilon_B = \hbar^2(2\pi/b)^2/(2m^*_{GaAs})$ is of the order of the conduction band width, $b = 5.65$ Å is the lattice constant of the unit cell and m^*_{GaAs} is the electron effective mass of GaAs.

The perturbed density of states can be calculated from the imaginary part of the Green's function and is given by the expression

$$\rho(E) = \frac{1}{\pi}\,\mathrm{Im}\sum_{\mathbf{k}} G_{\mathbf{kk}}(E) = \frac{1}{\pi}\int \rho_0\left(E_{\mathbf{k}}^C\right)\mathrm{Im}[G_{\mathbf{kk}}(E)]\,\mathrm{d}E_{\mathbf{k}}^C. \tag{11}$$

The integration converges rapidly with $E_{\mathbf{k}}^C$ in a small range that is proportional to x. The calculated perturbed density of states for $GaAs_{1-x}N_x$ with several small values of x is shown in figure 11. Note that the anticrossing interaction leads to

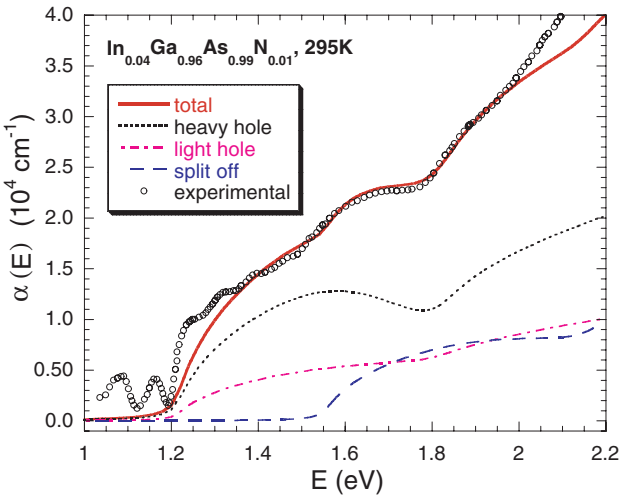

Figure 12. Calculated optical absorption coefficient in comparison with room-temperature experimental data [44] for free-standing $In_{0.04}Ga_{0.96}As_{0.99}N_{0.01}$. The oscillations below the absorption edge are due to Fabry–Perot interference.

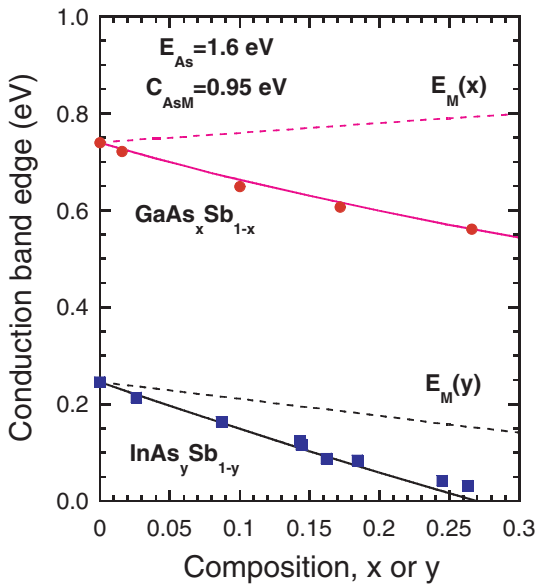

Figure 13. Energy of the conduction band edge in $GaAs_xSb_{1-x}$ [46] and $InAs_ySb_{1-y}$ [47]. The energies are relative to the valence band maximum of GaSb. The solid lines are calculated using the BAC model. $E_M(x)$ and $E_M(y)$ represent the energies of the conduction band minimum obtained from the virtual crystal approximation.

a considerable redistribution of the electronic states in the conduction band. The most striking feature of the density of states curves is the clearly seen gap between E_+ and E_- that evolves with increasing N content.

In order to illustrate the effect of the state broadening on the optical properties, we consider the spectral dependence of the interband absorption in $In_yGa_{1-y}As_{1-x}N_x$ alloys. The optical absorption coefficient due to the transitions from the valence bands to the restructured conduction bands can be written in the form of the joint density of states as

$$\alpha(E) \propto \frac{1}{E}\sum_v \int \rho_0\left(E^C_{\mathbf{k}}\right) \mathrm{Im}\left[G_{\mathbf{kk}}\left(E + E^v_{\mathbf{k}}\right)\right] \mathrm{d}E^C_{\mathbf{k}}. \quad (12)$$

In this expression, the sum over v represents the sum of the contributions from the heavy-hole, the light-hole and the spin–orbit split-off valence bands. Assuming parabolic forms for the dispersions of the valence bands near the Brillouin zone centre, we have calculated the optical absorption for $In_{0.04}Ga_{0.96}As_{0.99}N_{0.01}$ for which experimental results are available [46]. The comparison between the calculation and the experimental data is shown in figure 12. In the calculation, the only parameter that has been adjusted is the prefactor β used to scale the energy broadening. The best fitting with the experimental data is obtained with $\beta = 0.22$. The calculation clearly reproduces the two bumps on the absorption curve, i.e., one starting at ∼1.8 eV due to the onset of the transitions from the heavy-hole and light-hole valence bands to E_+, and one starting at ∼1.5 eV due to the onset of the transition from the split-off valence band to E_-. The more rapid rise of the experimental data at the absorption edge near 1.2 eV is most likely due to the continuum exciton absorption effect, which is not considered in the calculation.

4. Band anticrossing in other group III–V alloys

The band anticrossing model has explained successfully the strong bandgap bowing of all III–V–N HMAs. It should be emphasized that these alloys belong to a much broader class of materials. It has been shown recently that it includes group II–VI–O alloys in which highly electronegative O partially replaces more metallic group VI elements. Large band anticrossing effects were observed in $Cd_{1-y}Mn_yO_xTe_{1-x}$ with less than one per cent of oxygen [47]. Because of the high electronegativity of N and O atoms, both group III–V–N and group II–VI–O alloys represent extreme cases of HMAs in which the band anticrossing interaction leads to dramatic changes of the conduction band structure. There are, however, many of the III–V or II–VI alloys formed of anions with a smaller but still significant electronegativity difference. For example, it has been shown that the composition and pressure dependencies of the energy gap of $ZnTe_{1-x}S_x$ and $ZnTe_{1-y}Se_y$ can be described well by an anticrossing interaction of the localized levels of S and Se, respectively, with the extended states of the ZnTe matrix [19]. The effects of the anticrossing are clearly observed despite much smaller electronegativity difference of 0.4 for $ZnTe_{1-x}S_x$ and 0.3 for $ZnTe_{1-y}Se_y$ alloys.

It is well known that large bandgap bowings are observed in all group III–Sb alloys in which metallic Sb is replaced by either P or As. An interesting question arises: could the strong bowings also be explained by the band anticrossing interaction? Figure 13 shows the composition dependence of the energy of the conduction band edge in $GaAs_xSb_{1-x}$ [48] and $InAs_ySb_{1-y}$ [49] along with the results of calculations based on the BAC model. The calculations account well for the conduction band shifts assuming the energy of the localized As level lies at 1.6 eV above the valence band of GaSb and the coupling constant is 0.95 eV. The band anticrossing effects in these materials are significantly weaker compared with III–N–V alloys because of smaller electrongativity difference of 0.2 between Sb and As.

Somewhat larger anticrossing effects are expected for III–V alloys in which Sb with electronegativity of 1.8 is partially replaced by P with electronegativity of 2.1. Such

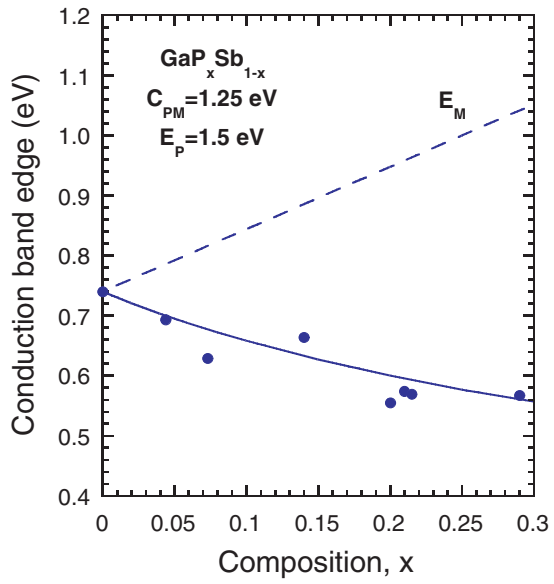

Figure 14. Conduction band minimum as function of composition in GaP_xSb_{1-x}. The points represent experimental data of [48]. The solid line shows the results of calculations with E_M representing the conduction band edge obtained within the virtual crystal approximation.

alloys containing P and Sb are difficult to synthesize because of a large immiscibility. A successful synthesis of GaP_xSb_{1-x} has shown that this alloy system exhibits a large bandgap bowing [50]. The energy of the conduction band edge as function of the P content is shown in figure 14. As expected, the anticrossing effects are more pronounced in this case than in the case of $GaAs_xSb_{1-x}$ or $InAs_ySb_{1-y}$ alloys. Note that there is quite a large deviation of the conduction band energy from the prediction of the VCA represented by E_M. Again, calculations based on the BAC model account very well for the downward shift of the conduction band edge.

5. Summary

In this paper we have reviewed the theoretical origin and resultant effects of band anticrossing between localized impurity states and the extended band states of the host in highly electronegativity-mismatched semiconductor alloys. Some important experimental results of $GaAs_{1-x}N_x$, $InP_{1-x}N_x$, and $GaP_{1-x}N_x$ have been discussed in the context of the band anticrossing model. It is demonstrated that the band anticrossing model can account successfully for the unusual behaviour of the highly mismatched alloys. The band anticrossing interaction does not only exist between the localized states and the conduction band near the Brillouin zone centre, but it also extends to the zone edge. As examples for the generality of the application of the band anticrossing model, we have shown that the large bowing parameters observed in group III–V alloys with As or P substituting Sb can also be explained by the interaction between localized As or P levels and the extended conduction band states of the semiconductor matrix.

Acknowledgments

J Wu acknowledges the Berkeley Fellowship from the University of California, Berkeley. We wish to gratefully acknowledge collaborations with Dr K M Yu, Dr J W Ager, Professor E E Haller, Dr J F Geisz, Dr Skierbiszewski and Professor C W Tu. The work at Lawrence Berkeley National Laboratory is part of the project on the 'Photovoltaic Materials Focus Area' in the DOE Centre of Excellence for the Synthesis and Processing of Advanced Materials, and was supported by the Director, Office of Science, Office of Basic Energy Sciences, Division of Materials Sciences of the US Department of Energy under Contract No DE-AC03–76SF00098.

References

[1] Van Vechten J A and Bergstresser T K 1970 *Phys. Rev.* B **1** 3351
[2] Hill R and Richardson D 1971 *J. Phys.* C **4** L289
[3] Weyers M, Sato M and Ando H 1992 *Japan. J. Appl. Phys.* **31** L853
Uesugi K, Marooka N and Suemune I 1999 *Appl. Phys. Lett.* **74** 1254
[4] Skierbiszewski C *et al* 2000 *Appl. Phys. Lett.* **76** 2409
[5] Kurtz S R, Allerman A A, Seager C H, Sieg R M and Jones E D 2000 *Appl. Phys. Lett.* **77** 400
Geisz J F, Friedman D J, Olson J M, Kurtz S R and Keyes B M 1998 *J. Cryst. Growth* **195** 401
[6] Baillargeon N, Cheng K Y, Hofler G F, Pearah P J and Hsieh K C 1992 *Appl. Phys. Lett.* **60** 2540
[7] Bi W G and Tu C W 1996 *J. Appl. Phys.* **80** 1934
[8] Harmand J C, Ungaro G, Ramos J, Rao E V K, Saint-Girons G, Teissier R, Le Roux G, Largeau L and Patriarche G 2001 *J. Cryst. Growth* **227–228** 553
[9] Murdin B N *et al* 2001 *Appl. Phys. Lett.* **78** 1558
[10] Van Vechten J A and Bergstresser T K 1970 *Phys. Rev.* B **8** 3351
[11] Sakai S, Ueta Y and Terauchi Y 1993 *Japan. J. Appl. Phys.* **32** 4413
[12] Wei Su-Huai and Zunger A 1996 *Phys. Rev. Lett.* **76** 664
[13] Jones E D, Modine N A, Allerman A A, Kurtz S R, Wright A F, Tozer S T and Wei X 1999 *Phys. Rev.* B **60** 4430
[14] Mattila T, Wei Su-Huai and Zunger A 1999 *Phys. Rev.* B **60** R11 245
[15] Wang Lin-Wang 2001 *Appl. Phys. Lett.* **78** 1565
Szwacki N G and Boguslawski P 2001 *Phys. Rev.* B **64** 161201
[16] Al-Yacoub A and Bellaiche L 2000 *Phys. Rev.* B **62** 10 847
[17] Zhang Y, Mascarenhas A, Xin H P and Tu C W 2001 *Phys. Rev.* B **63** 161303
[18] Shan W, Walukiewicz W, Ager J W III, Haller E E, Geisz J F, Friedman D J, Olson J M and Kurtz S R 1999 *Phys. Rev. Lett.* **82** 1221
[19] Walukiewicz W, Shan W, Yu K M, Ager J W III, Haller E E, Miotkowski I, Seong M J, Alawadhi H and Ramdas A K 2000 *Phys. Rev. Lett.* **85** 1552
[20] Shan W, Walukiewicz W, Yu K M, Wu J, Ager J W III, Haller E E, Xin H P and Tu C W 2000 *Appl. Phys. Lett.* **76** 3251
[21] Yu K M, Walukiewicz W, Shan W, Ager J W III, Wu J, Haller E E, Geisz J F, Friedman D J and Olson J M 2000 *Phys. Rev.* B **61** R13337
[22] Anderson P W 1961 *Phys. Rev.* **124** 41
[23] Kocharyan A N 1986 *Soc. Phys. Solid State* **28** 6
[24] Ivanov M A and Yu G Pogorelov 1979 *Sov. Phys.–JETP* **49** 510
Ivanov M A and Yu G Pogorelov 1985 *Sov. Phys.–JETP* **61** 1033
[25] Wu J, Walukiewicz W and Haller E E 2002 *Phys. Rev.* B **65** 233210

[26] Harold P Hjalmarson, Vogl P, Wolford D J and John D Dow 1980 *Phys. Rev. Lett.* **44** 810
[27] Wolford D J, Bradley J A, Fry K and Thompson J 1984 *Physics of Semiconductors* ed J D Chadi and W A Harrison (New York: Springer)
[28] Hsu W Y, Dow J D, Wolford D J and Streetman B G 1977 *Phys. Rev.* B 16 1597
[29] Yonezawa Fumiko and Morigaki Kazuo 1973 *Prog. Theor. Phys.* **53** Supplement
[30] Elliott R J, Krumhansl J A and Leath P L 1974 *Rev. Mod. Phys.* **46** 465
[31] Liu Xiao, Pistol M-E, Samuelson L, Schwetlick S and Seifert W 1990 *Appl. Phys. Lett.* **56** 1451
[32] Lindsay A and O'Reilly E P 1999 *Solid State Commun.* **112** 443
[33] Keyes B M, Geisz J F, Dippo P C, Reedy R, Kramer C, Friedman D J, Kurtz Sarah R and Olson J M 1999 NCPV photovoltaics program review *AIP Conf. Proc.* **462** 511
[34] Malikova L, Pollak F H and Bhat R 1998 *J. Electron. Mater.* **27** 484
[35] Bhat R, Caneau C, Salamanca-Riba L, Bi W and Tu C 1998 *J. Cryst. Growth* **195** 427
[36] Shan W, Walukiewicz W, Ager J W III, Haller E E, Geisz J F, Friedman D J, Olson J M and Kurtz Sarah R 1999 *J. Appl. Phys.* **86** 2349
[37] Yu K M, Walukiewicz W, Wu J, Beeman J W, Ager J W III, Haller E E, Shan W, Xin H P, Tu C W and Ridgway M C 2001 *J. Appl. Phys.* **90** 2227
[38] Sun B Q, Jiang D S, Luo X D, Xu Z Y, Pan Z, Li L H and Wu R H 2000 *Appl. Phys. Lett.* **76** 2862
[39] Kitatani Takeshi, Kondow Masahiko, Kikawa Takeshi, Yazawa Yoshiaki, Okai Makoto and Uomi Kazuhisa 1999 *Japan. J. Appl. Phys.* **38** 5003
Tanaka S, Takahashi M, Moto A, Tanabe T, Takagishi S, Karatani K, Nakanishi T and Nakayama M 1998 *25th International Symposium on Compound Semiconductors (Nara, Japan)*
[40] Wu J, Shan W, Walukiewicz W, Yu K M, Ager J W III, Haller E E, Xin H P and Tu C W 2001 *Phys. Rev.* B **64** 85320
[41] Jones E D, Modine N A, Allerman A A, Fritz I J, Kurtz S R, Wright A F, Tozer S T and Wei Xing 1999 *Proc. 195th Electrochem. Soc. Meeting (Seattle, WA 99–11)* 170
[42] Hetterich M, Dawson M D, Egorov A Yu, Bernklau D and Riechert H 2000 *Appl. Phys. Lett.* **76** 1030
[43] Wu J, Walukiewicz W, Yu K M, Ager J W III, Haller E E, Hong Y G, Xin H P and Tu C W 2002 *Phys. Rev.* B **65** 241303(R)
[44] Seong M J, Mascarenhas A and Geisz J F 2001 *Appl. Phys. Lett.* **79** 1297
[45] Perkins J D, Mascarenhas A, Geisz J F and Friedman D J 2001 *Phys. Rev.* B **64** 121301
[46] Perlin P, Wisniewski P, Skierbiszewski C, Suski T, Kaminska E, Subramanya S G, Weber E R, Mars D E and Walukiewicz W 2000 *Appl. Phys. Lett.* **76** 1279
[47] Yu K M, Walukiewicz W, Wu J, Beeman J W, Ager J W III, Haller E E, Miotkowski I, Ramdas A K and Becla P 2002 *Appl. Phys. Lett.* **80** 1571
[48] Thomas M B, Coderre W M and Wooley J 1970 *Phys. Status Solidi* A **2** K141
[49] Coderre W M and Wooley J C 1968 *Can. J. Phys.* **46** 1207
[50] Loualiche S, Le Corre A, Salaun S, Caulet J, Lambert B, Gauneau M, Lecrosnier D and Deveaud B 1991 *Appl. Phys. Lett.* **59** 423
Jou M J, Cherng Y T, Jen H R and Stringfellow G B 1987 *Appl. Phys. Lett.* **52** 549